

The Young's modulus of high-aspect-ratio carbon/carbon nanotube composite microcantilevers by experimental and modeling validation

Peng Zhou, Xiao Yang, Liang He, Zhimeng Hao, Wen Luo, Biao Xiong, Xu Xu, Chaojiang Niu, Mengyu Yan, and Liqiang Mai

Citation: [Applied Physics Letters](#) **106**, 111908 (2015); doi: 10.1063/1.4915514

View online: <http://dx.doi.org/10.1063/1.4915514>

View Table of Contents: <http://scitation.aip.org/content/aip/journal/apl/106/11?ver=pdfcov>

Published by the [AIP Publishing](#)

Articles you may be interested in

[An arbitrary strains carbon nanotube composite piezoresistivity model for finite element integration](#)
Appl. Phys. Lett. **102**, 011909 (2013); 10.1063/1.4774294

[Young's modulus measurement of two-photon polymerized micro-cantilevers by using nanoindentation equipment](#)
J. Appl. Phys. **112**, 094906 (2012); 10.1063/1.4764330

[Effect of filament aspect ratio on the dielectric response of multiwalled carbon nanotube composites](#)
J. Appl. Phys. **109**, 094109 (2011); 10.1063/1.3569596

[Conductivity of carbon nanotube polymer composites](#)
Appl. Phys. Lett. **90**, 033116 (2007); 10.1063/1.2432237

[Electromagnetic wave propagation in dense carbon nanotube arrays](#)
J. Appl. Phys. **99**, 076106 (2006); 10.1063/1.2186972

The advertisement features a photograph of the Model PS-100 cryogenic probe station, a complex piece of scientific equipment with various mechanical components and a probe. The background is a gradient of blue. On the left, the text 'Model PS-100' is in a large, bold, white font, with 'Tabletop Cryogenic Probe Station' below it in a smaller white font. On the right, the 'Lake Shore CRYOTRONICS' logo is displayed, with 'Lake Shore' in a large, white, serif font and 'CRYOTRONICS' in a smaller, white, sans-serif font below it. Below the logo, the tagline 'An affordable solution for a wide range of research' is written in a white, italicized serif font.



The Young's modulus of high-aspect-ratio carbon/carbon nanotube composite microcantilevers by experimental and modeling validation

Peng Zhou,^{a)} Xiao Yang,^{a)} Liang He,^{b)} Zhimeng Hao, Wen Luo, Biao Xiong, Xu Xu, Chaojiang Niu, Mengyu Yan, and Liqiang Mai^{b)}

State Key Laboratory of Advanced Technology for Materials Synthesis and Processing, Wuhan University of Technology, Wuhan 430070, People's Republic of China

(Received 16 February 2015; accepted 8 March 2015; published online 18 March 2015)

This paper reports the Young's modulus of a carbon nanotube (CNT)-reinforced carbon/CNT (C/CNT) composite microcantilevers measured by laser Doppler vibrometer and validated by finite element method. Also, the microfabrication process of the high-aspect-ratio C/CNT microcantilever arrays based on silicon micromolding and pyrolysis is presented in detail. With the in-plane natural resonant frequencies of the microcantilevers measured by a laser Doppler vibrometer, a single degree of freedom (SDoF) model based on Euler-Bernoulli (E-B) beam theory is used to calculate the Young's modulus of this composite. To figure out whether this SDof model can be applied to these composite microcantilevers, the finite element (FE) simulation of these microcantilevers was performed. The Young's modulus of C/CNT composite microcantilevers fabricated by the pyrolysis process at 600 °C is 9391 MPa, and a good agreement between the results from experiments and FE simulation is obtained. © 2015 AIP Publishing LLC. [<http://dx.doi.org/10.1063/1.4915514>]

The microcantilevers have been widely utilized for micro electro mechanical systems (MEMSs) such as force sensors, biosensors, and microactuators.¹⁻⁵ In many applications of microcantilevers, high vibrational frequency is required, especially for the micro/nano devices with ultra-high sensitivity or resolution. Various microcantilevers based on materials with high stiffness and wide applications were fabricated and investigated. For example, silicon based materials (silicon, polysilicon, and silicon carbide⁶⁻⁸) are the most investigated materials for the applications in microcantilevers due to the maturity of silicon based micro machining technologies. The microfabrication processes of silicon microcantilevers can be easily integrated with existing semiconductor microfabrication processes, such as lithography, metal film deposition, lift-off, dry etching, and wet etching techniques, which have been applied in the fabrication of silicon microcantilevers.

Generally, in these processes, the microcantilever regions patterned by photolithography and SiO₂ layers formed by dry oxidation or originally buried in silicon-on-insulator (SOI) wafers are served as protective patterns for dry/wet etching of the silicon.^{6,7} Furthermore, the remaining SiO₂ in the surrounding areas of these regions are striped by buffered HF (BHF) solution or other dry etching methods. The silicon microcantilevers can be easily lined up by high-yield microfabrication process.⁷ However, the fabrication of high-aspect-ratio microcantilever arrays based on other materials is an emerging challenge since the synthesis of some materials cannot be easily integrated with the microfabrication process. Besides, low wear resistance, low toughness, and low alkali corrosion resistance limit the applications of silicon microcantilevers. Therefore, carbon based materials which possess the chemical

inertness, relatively high elastic modulus and low density, become an important kind of alternative materials for microcantilevers.⁹⁻¹⁴ In the previous researches, freestanding and diamond-like carbon microcantilevers based on amorphous carbon films by isotropic wet etching were fabricated and characterized.⁹⁻¹² Also, the photoresist-derived pyrolysis carbon and other amorphous carbon have been widely investigated for applications in MEMSs since their unique physical properties are complementary to silicon, and their fabrication process can be compatible with microfabrication technologies.^{15,16}

Some one-dimensional nanostructures (nanofibers, nanowires, and nanorods) can be utilized as high-performance reinforcements for the composite materials with enhanced physical properties.¹⁷⁻¹⁹ In recent years, carbon nanotubes (CNTs) have been investigated and utilized as reinforcing agents in micro/nano structures due to their high mechanical strength and low density.²⁰ An important increase of the tensile modulus and toughness of matrices has been reported for the random dispersion of single-walled CNTs (SWCNTs) or multi-walled CNTs (MWCNTs). For example, the strain energy density and the ductility of polyethylene increased by ~150% and ~140% with a loading of 1 wt. % MWCNTs randomly distributed.²⁰ Therefore, the integration of CNTs into carbon based micro/nano structures and devices is of great significance.

A reported fabrication process based on Si micromolding and pyrolysis^{21,22} is employed to fabricate high-aspect-ratio carbon/CNT (C/CNT) microcantilevers in this research. Also, the detailed Young's modulus of these microcantilevers is investigated by measuring their resonant frequencies, and a single degree of freedom (SDof) model based on Euler-Bernoulli (E-B) beam theory that provides an analytical determination is applied to calculate the Young's modulus of the composite microcantilevers.^{23,24} Besides, a three-dimensional finite element (FE) model is built to verify the accuracy of the analytical results.^{25,26} The experimental and

^{a)}P. Zhou and X. Yang contributed equally to this work.

^{b)}Authors to whom correspondence should be addressed. Electronic addresses: hel@whut.edu.cn and mlq518@whut.edu.cn.

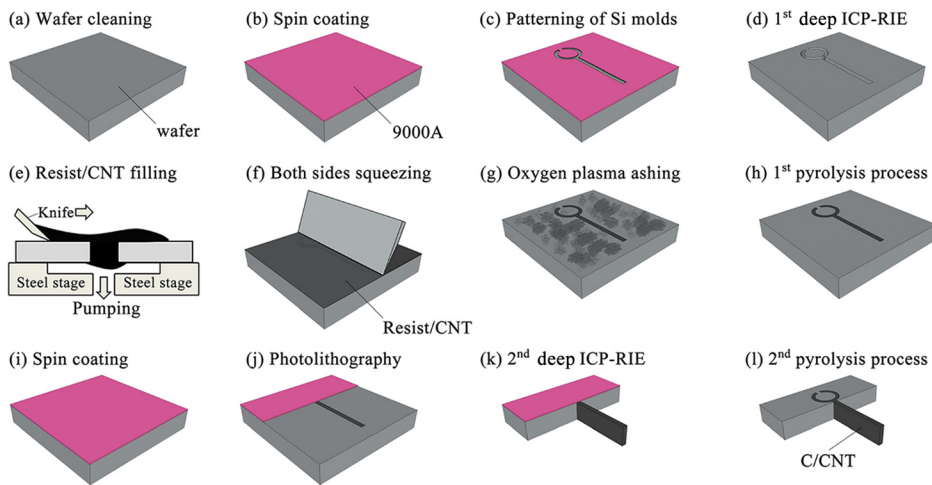


FIG. 1. Fabrication process of C/CNT composite microcantilevers.

simulation results from these cantilever geometries are in good agreement, which validates the Young's modulus of the C/CNT composite microcantilevers fabricated by this process.

In our research, C/CNT microcantilevers with high-aspect-ratio (height: $340\ \mu\text{m}$ and width: $50\ \mu\text{m}$) were fabricated and characterized for their resonant frequencies. As the fabrication process including Si micromolding and deep inductive coupled plasma reactive ion etching (ICP-RIE) shown in Figure 1, the C/CNT microcantilevers were fabricated from SU-8 50 negative photoresist (MicroChem Corp.) mixed with 1 wt. % MWCNTs (Nano Carbon Technologies Corp.). The SU-8 50 possesses suitable viscosity for the fabrication process of this research. Ultrasonic irradiation was employed to prepare the resist/CNT nanocomposite, by taking advantage of its multiple effects, such as dispersion, initiation, and activation, to guarantee homogeneous dispersion and stabilization of MWCNTs in SU-8 50 matrix.²¹

In the fabrication process, the silicon substrates ($400\ \mu\text{m}$, (100)-oriented, n-type) were cleaned by typical RCA cleaning process. Then, the silicon substrates were immersed into the 1% HF solution for 15 s followed by baking at $145\ ^\circ\text{C}$ for 30 min. After the cleaning and baking, a spin coating of photoresist was carried out, and the patterning of the photoresist was conducted by photolithography. The Si micromolds were fabricated by deep ICP-RIE process. Afterwards, these Si micromolds were filled with resist/CNT composite by back-side pumping, and the remained composite on the both sides of Si surface was removed by squeezing and oxygen plasma ashing treatment, therefore, the resist/CNT on the silicon substrate was completely removed. Then, the resist/CNT was converted to C/CNT composite microstructures by a two-step pyrolysis process in a quartz-tube furnace under N_2 atmosphere. The samples were initially heated at $5\ ^\circ\text{C}/\text{min}$ rate from room temperature to $400\ ^\circ\text{C}$, and held at this temperature for 60 min. The obtained samples were eventually cooled down slowly to the room temperature under N_2 atmosphere. The photolithography and ICP-RIE process were conducted again to fabricate hybrid silicon/composite microstructures and release the composite microcantilevers. These microcantilevers were annealed at higher temperature ($600\ ^\circ\text{C}$) for 60 min with the heating rate of $5\ ^\circ\text{C}/\text{min}$ from room temperature to $600\ ^\circ\text{C}$ under N_2 atmosphere during the second pyrolysis

process. Eventually, the samples were also cooled down slowly to the room temperature under N_2 atmosphere. Therefore, the resist/CNT was converted to C/CNT composite by this two-step pyrolysis process, and the fabrication process was completed.

The morphology of the C/CNT composite microcantilevers was characterized by field emission scanning electron microscopy (FE-SEM), as shown in Fig. 2. The released high-aspect-ratio microcantilevers with different sizes have been realized by this fabrication process. The aspect ratio of ~ 7 can be achieved by this process including two-step pyrolysis. The vertical shrinkage on the surface can be observed, which is generated by the densification of the polymer structures induced by the removal of noncarbon species during pyrolysis process. The lateral shrinkage from the SEM images is unapparent, which is consistent with the results of carbon micro/nano structures derived from different precursors. The result is attributed to the initial strong adhesive force between the resist/CNT composite and the silicon side walls.

The structure/volume shrinkage and weight loss are usually involved in carbonization of the microstructures due to the removal of the noncarbon species during the pyrolysis process.²⁴ Therefore, the density of C/CNT composite is estimated

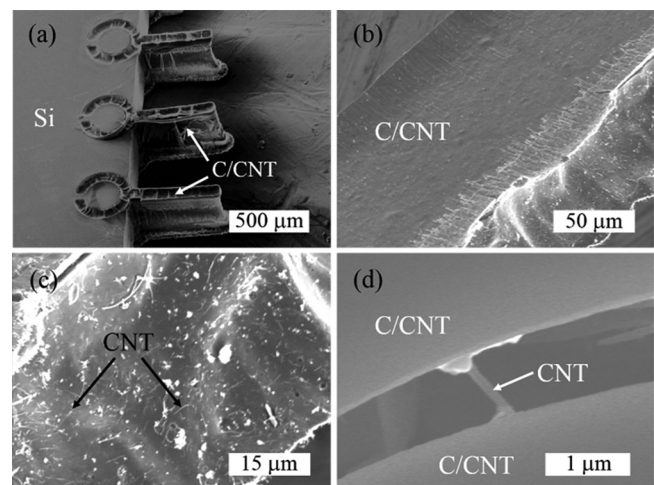


FIG. 2. SEM images of the fabricated C/CNT composite microcantilevers, (a) tilt view of microcantilevers array; (b) tilt view of the surface of one microcantilever; (c) magnified view of the surface of one microcantilever; and (d) a CNT in the fracture section of C/CNT film.

from the weight and volume of the C/CNT films fabricated by the same pyrolysis process under same conditions. The random distribution of CNTs on the surface of C/CNT microcantilevers is observed, as shown in Fig. 2(c), and the single CNT in the fracture section of the C/CNT film also verify the distribution of CNTs in matrix. The weight of the composite film before and after pyrolysis process are measured by the digital electrobalance with a $0.1 \mu\text{N}$ resolution, and the volume of the composite film is estimated from the area and thickness by surface profiler. According to our measurement, the weight shrinkage and volume shrinkage were 40.2% and 64.8%, respectively.²¹ Therefore, 1 wt. % MWCNT in SU-8 50 became 1.67 wt. % in the pyrolysis process since the weight of the MWCNTs did not change. The density of the composite microstructures is $2.06 \pm 0.06 \text{ g/cm}^3$.²¹

For the investigation of the Young's modulus of as-fabricated microcantilevers, a laser Doppler vibrometer is utilized to measure their natural resonant frequencies. As shown in Fig. 3, these microcantilevers are placed on the sample stage in a vacuum chamber, the laser beam of the laser Doppler vibrometer is focused at the vertical wall of the microcantilever, and the flexural modes of lateral vibration were measured. The Young's modulus of the composite is estimated from the resonant frequencies of microcantilevers. For a SDoF model, these microcantilevers are considered to be ideally clamped E-B cantilever beams. And the mass load of a cantilever is simplified to a point load at the free end. The microcantilevers can thus be considered to execute simple harmonic motion when they are in a vacuum chamber. For the resonant frequency of a rectangle cantilever, it can be calculated by Eq. (1), where K is the spring constant, and m^* is the effective mass of the cantilever. K and m^* can be derived from Eqs. (2) and (3), respectively, where E is the Young's modulus of the composite, t is the width of the microcantilever, L is the length of the microcantilever, n is a geometry constant of 0.24, and ρ is the mass density of the composite^{23,24}

$$f = \frac{\sqrt{K/m^*}}{2\pi}, \quad (1)$$

$$K = \frac{Et^3w}{4l^3}, \quad (2)$$

$$m^* = nptwl. \quad (3)$$

By using Eqs. (1)–(3), the Young's modulus of the C/CNT composite microcantilever is given by the following equation:

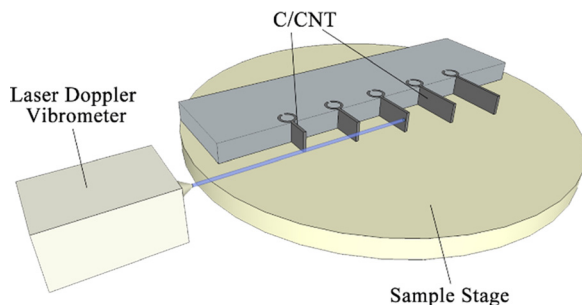


FIG. 3. Schematic view of the resonant frequencies measurement including the C/CNT composite microcantilevers array, the sample stage, and a laser Doppler vibrometer.

$$E = \frac{16n\rho\pi^2}{t^2} \times f^2 l^4. \quad (4)$$

With this SDoF model for the determination of the Young's modulus, the least squares method was applied to extract the Young's modulus using the measured resonant frequencies of the microcantilevers and their real geometric dimensions. According to our calculation, the Young's modulus of the C/CNT composite is 9391 MPa.

To verify the adequacy of the SDoF model for the determination of the Young's modulus, a three-dimensional FE simulation of microcantilevers was performed by using a commercial package *ANSYS workbench*, as shown in Fig. 4.^{25,26} In this simulation, the values of the Young's modulus, Poisson's ratio, and mass density of the composite are $E = 9391 \text{ MPa}$, $\nu = 0.15$, and $\rho = 2.06 \text{ g/cm}^3$, respectively. All-Hexahedral mesh was generated and the size of the element for meshing was program-controlled. The regions of the microcantilevers contact with the Si micromolds were defined as a fixed support, which means the boundary condition prevents the contact faces from moving or deforming.

The calculated first-order model frequencies of the microcantilevers by FE simulation are listed in Fig. 5. Experimental results of the resonant frequencies of the C/CNT composite are in good agreement with the results obtained from the three-dimensional FE analysis, which demonstrates that the determination derived from the SDoF model based on E-B beam theory is capable for calculating the Young's modulus of these microcantilevers. Therefore, the Young's modulus derived from E-B beam theory and calculation is believable. The experimental resonant frequencies of the microcantilevers, the E-B prediction, and the simulation results are presented in Fig. 5 with the detailed geometric dimensions. The results from FE simulation are always lower than that of the statistical SDoF values. The voids generated from the fabrication process in the composite microcantilevers result in an overestimation of density of these microcantilevers, and the FE model, which is more accurate, can be more sensitive to this overestimation.

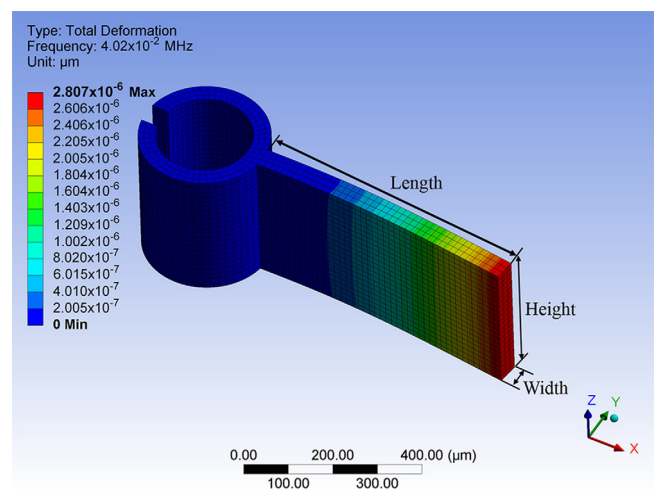


FIG. 4. View of the FE simulation results of the microcantilever with length of $650 \mu\text{m}$. The values of the Young's modulus, Poisson's ratio, and mass density of the composite illustrated here are $E = 9391 \text{ MPa}$, $\nu = 0.15$, and $\rho = 2.06 \text{ g/cm}^3$, respectively.

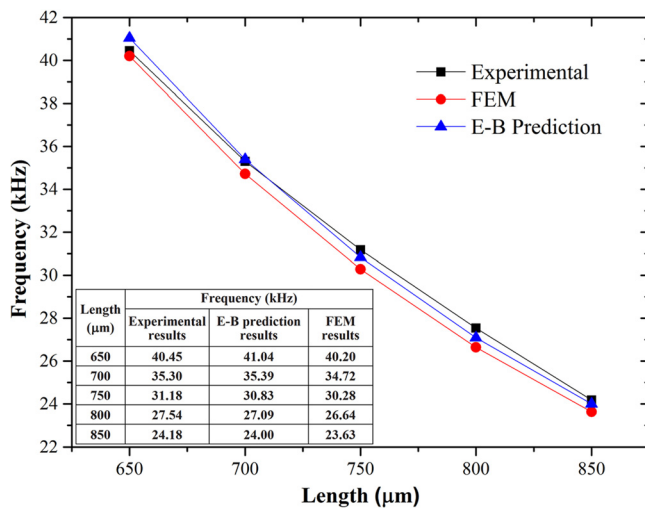


FIG. 5. The experimental, E-B prediction and FE simulation results of the C/CNT composite microcantilevers with various lengths (width = 50 μm).

The high-aspect-ratio C/CNT composite microcantilevers were fabricated by silicon micromolding combined with two-step pyrolysis process. The Young's modulus of these C/CNT composite microcantilevers is calculated from their natural resonant frequencies with SDoF model based on E-B beam theory and validated by the FE simulations. The results from theoretical analysis and numerical simulation are in good agreement. Our microfabrication process for these high-aspect-ratio microcantilevers and reasonable theoretical calculations validated by FE simulations have great potential for the development and wide applications of high-performance microcantilevers.

This work was supported by the National Basic Research Program of China (Nos. 2013CB934103 and 2012CB933003), the National Natural Science Fund for Distinguished Young Scholars (No. 51425204), and the Fundamental Research Funds for the Central Universities (WUT: 2014-IV-062 and 2014-IV-147). Thanks to Professor T. Ono of Tohoku University for strong support and stimulating discussion.

- ¹G. Stemme, *J. Micromech. Microeng.* **1**, 113 (1991).
- ²V. Snitka, R. D. Rodrigues, and V. Lendraitis, *Microelectron. Eng.* **88**, 2759 (2011).
- ³V. Seena, A. Fernandes, P. Pant, S. Mukherji, and V. R. Rao, *Nanotechnology* **22**, 295501 (2011).
- ⁴D. W. Lee, T. Ono, and M. Esashi, *Sens. Actuators, A* **83**, 11 (2000).
- ⁵I.-C. Chen, L.-H. Chen, A. Gapin, S. Jin, L. Yuan, and S.-H. Liou, *Nanotechnology* **19**, 075501 (2008).
- ⁶H. J. H. Chen and C. S. Hung, *Nanotechnology* **18**, 355305 (2007).
- ⁷X. X. Li, T. Ono, Y. L. Wang, and M. Esashi, *Appl. Phys. Lett.* **83**, 3081 (2003).
- ⁸J. L. Yang, T. Ono, and M. Esashi, *Sens. Actuators, A* **82**, 102 (2000).
- ⁹D. Sheeja, B. K. Tay, L. J. Yu, D. H. C. Chua, W. I. Milne, J. Miao, and Y. Q. Fu, *Diamond Relat. Mater.* **12**, 1495 (2003).
- ¹⁰D. Sheeja, B. K. Tay, S. P. Lau, L. J. Yu, J. M. Miao, H. C. Chua, and W. I. Milne, *Sens. Actuators, B* **98**, 275 (2004).
- ¹¹J.-Y. Igaki, K.-I. Nakamatsu, R. Kometani, K. Kanda, Y. Haruyama, T. Kaito, and S. Matsui, *J. Vac. Sci. Technol., B* **24**(6), 2911 (2006).
- ¹²D. H. C. Chua, B. K. Tay, P. Zhang, E. H. T. Teo, L. T. W. Lim, S. O'Shea, J. Miao, and W. I. Milne, *Diamond Relat. Mater.* **13**, 1980 (2004).
- ¹³E. D. Feng and R. E. Jones, *Phys. Rev. B* **83**, 195412 (2011).
- ¹⁴M. Lu, M.-W. Jang, S. A. Campbell, and T. H. Cui, *J. Vac. Sci. Technol., B* **28**(3), 522 (2010).
- ¹⁵J. A. Lee, K.-C. Lee, S. I. Park, and S. S. Lee, *Nanotechnology* **19**, 215302 (2008).
- ¹⁶H.-S. Min, B. Y. Park, L. Taherabadi, C. L. Wang, Y. Yeh, R. Zaouk, M. J. Madou, and B. Dunn, *J. Power Sources* **178**, 795 (2008).
- ¹⁷C. Balázs, B. Fényi, N. Hegman, Z. Kövér, F. Wéber, Z. Vértessy, Z. Kónya, I. Kiricsi, L. P. Biró, and P. Arató, *Composites, Part B* **37**, 418 (2006).
- ¹⁸F. T. Fisher, R. D. Bradshaw, and L. C. Brinson, *Appl. Phys. Lett.* **80**(24), 4647 (2002).
- ¹⁹K. Inaba, K. Saida, P. Ghosh, K. Matsubara, M. Subramanian, A. Hayashi, Y. Hayashi, M. Tanemura, M. Kitazawa, and R. Ohta, *Carbon* **49**, 4191 (2011).
- ²⁰S. L. Ruan, P. Gao, X. G. Yang, and T. X. Yu, *Polymer* **44**, 5643 (2003).
- ²¹L. He, M. Toda, Y. Kawai, H. Miyashita, M. Omori, T. Hashida, R. Berger, and T. Ono, *Microsyst. Technol.* **20**(2), 201 (2014).
- ²²L. He, M. Toda, Y. Kawai, M. F. Sarbi, M. Omori, T. Hashida, and T. Ono, *IEEEJ Trans. Sens. Micromach.* **132**(11), 425 (2012).
- ²³J. P. Cleveland, S. Manne, D. Bocek, and P. K. Hansma, *Rev. Sci. Instrum.* **64**, 403 (1993).
- ²⁴B. Ilic, S. Krylov, and H. G. Craighead, *J. Appl. Phys.* **108**, 044317 (2010).
- ²⁵L. Xiong, Q. Zhou, Y. Wu, and P. Chen, *Mech. Syst. Sig. Process.* **50–51**, 227 (2015).
- ²⁶M. L. Chandravanshi and A. K. Mukhopadhyay, in *Proc. ASME IMECE* (2013), p. 62533.